MIT Open Access Articles

The LHCb trigger and its performance in 2011

The LHCb trigger and its performance in 2011

R. Aaij,[o] J. Albrecht,[m] F. Alessio,[m] S. Amato,[a] E. Aslanides,[d] I. Belyaev,[i]
M. van Beuzekom,[o] E. Bonaccorsi,[m] R. Bonnefoy,[c] L. Brarda,[m] O. Callot,[e]
M. Cattaneo,[m] H. Chanal,[c] M. Chebbi,[m] X. Cid Vidal,[l] M. Clemencic,[m] J. Closier,[m]
V. Coco,[o] J. Cogan,[d] O. Deschamps,[c] H. Dijkstra,[m,1] C. Drancourt,[b] R. Dzhelyadin,[j]
M. Frank,[m] M. Gandelman,[a] C. Gaspar,[m] V.V. Gligorov,[m] C. Göbel,[v]
L.A. Granado Cardoso,[m] Yu. Guz,[j] C. Haen,[m] J. He,[e] E. van Herwijnen,[m]
W. Hulsbergen,[o] R. Jacobsson,[m] B. Jost,[m] T.M. Karbach,[m] U. Kerzel,[m]
P. Koppenburg,[o] G. Krocker,[f] C. Langenbruch,[m] I. Lax,[g] R. Le Gac,[d] R. Lefèvre,[c]
J. Lefrancois,[e] O. Leroy,[d] L. Li Gioi,[c] G. Liu,[m] F. Machefert,[e] I.V. Machikhiliyan,[b,i]
M. Magne,[c] G. Mancinelli,[d] U. Marconi,[g] A. Martín Sánchez,[e] M.-N. Minard,[b]
S. Monteil,[c] N. Neufeld,[m] V. Niess,[c] S. Oggero,[o] A. Pérez-Calero Yzquierdo,[k]
P. Perret,[c] M. Perrin-Terrin,[d] B. Pietrzyk,[b] A. Puig Navarro,[n] G. Raven,[p] P. Robbe,[e]
H. Ruiz,[k] M.-H. Schune,[e] R. Schwemmer,[m] J. Serrano,[d] I. Shapoval,[q,m]
T. Skwarnicki,[u] B. Souza De Paula,[a] P. Spradlin,[r] S. Stahl,[f] V.K. Subbiah,[m]
S. T'Jampens,[b] F. Teubert,[m] C. Thomas,[t] M. Vesterinen,[m] M. Williams,[s,w] M. Witek,[h]
and A. Zvyagin[m]

[a]*Universidade Federal do Rio de Janeiro (UFRJ), Rio de Janeiro, Brazil*

[b]*LAPP, Université de Savoie, CNRS/IN2P3, Annecy-Le-Vieux, France*

[c]*Clermont Université, Université Blaise Pascal, CNRS/IN2P3, LPC, Clermont-Ferrand, France*

[d]*CPPM, Aix-Marseille Université, CNRS/IN2P3, Marseille, France*

[e]*LAL, Université Paris-Sud, CNRS/IN2P3, Orsay, France*

[f]*Physikalisches Institut, Ruprecht-Karls-Universität Heidelberg, Heidelberg, Germany*

[g]*Sezione INFN di Bologna, Bologna, Italy*

[h]*Henryk Niewodniczanski Institute of Nuclear Physics, Polish Academy of Sciences, Kraków, Poland*

[i]*Institute of Theoretical and Experimental Physics (ITEP), Moscow, Russia*

[j]*Institute for High Energy Physics (IHEP), Protvino, Russia*

[k]*Universitat de Barcelona, Barcelona, Spain*

[l]*Universidad de Santiago de Compostela, Santiago de Compostela, Spain*

[m]*European Organization for Nuclear Research (CERN), Geneva, Switzerland*

[1]Corresponding author.

^{n}*Ecole Polytechnique Fédérale de Lausanne (EPFL), Lausanne, Switzerland*

^{o}*Nikhef National Institute for Subatomic Physics, Amsterdam, The Netherlands*

^{p}*Nikhef National Institute for Subatomic Physics and VU University Amsterdam,*
Amsterdam, The Netherlands

^{q}*NSC Kharkiv Institute of Physics and Technology (NSC KIPT), Kharkiv, Ukraine*

^{r}*School of Physics and Astronomy, University of Glasgow, Glasgow, United Kingdom*

^{s}*Imperial College London, London, United Kingdom*

^{t}*Department of Physics, University of Oxford, Oxford, United Kingdom*

^{u}*Syracuse University, Syracuse, NY, United States*

^{v}*Pontifícia Universidade Católica do Rio de Janeiro (PUC-Rio), Rio de Janeiro, Brazil*[2]

^{w}*Massachusetts Institute of Technology, Cambridge, MA, United States*

E-mail: Hans.Dijkstra@cern.ch

ABSTRACT: This paper presents the design of the LHCb trigger and its performance on data taken at the LHC in 2011. A principal goal of LHCb is to perform flavour physics measurements, and the trigger is designed to distinguish charm and beauty decays from the light quark background. Using a combination of lepton identification and measurements of the particles' transverse momenta the trigger selects particles originating from charm and beauty hadrons, which typically fly a finite distance before decaying. The trigger reduces the roughly 11 MHz of bunch-bunch crossings that contain at least one inelastic pp interaction to 3 kHz. This reduction takes place in two stages; the first stage is implemented in hardware and the second stage is a software application that runs on a large computer farm. A data-driven method is used to evaluate the performance of the trigger on several charm and beauty decay modes.

---

[2]Associated to Universidade Federal do Rio de Janeiro (UFRJ), Rio de Janeiro, Brazil.

Contents

1 Introduction

The LHCb detector [1] is a single-arm spectrometer that has been optimised to perform flavour physics measurements at the LHC. LHCb has a pseudorapidity acceptance of $2 < \eta < 5$. The detector layout is shown in figure 1. It consists of a silicon vertex detector surrounding the pp interaction region (VELO); a silicon strip detector (TT); a dipole magnet; two Ring Imaging Cherenkov detectors (RICH 1&2); tracking detectors (T1–T3), which consist of silicon strip detectors (IT) near the beam and straw tubes (OT) further out; a calorimeter system consisting of a Scintillating Pad detector (SPD), an electromagnetic calorimeter with pre-shower (ECAL, PS) and a hadronic calorimeter (HCAL); and muon chambers (M1–M5).

The LHCb trigger uses all of the above sub-systems. Its architecture consists of two levels, the first level trigger (L0) and the High Level Trigger (HLT). L0 is implemented in hardware and uses input from the calorimeter and muon systems. L0 reduces the rate of crossings with at least one inelastic pp interaction to below 1.1 MHz, at which the whole detector can be read out. This maximum rate is imposed by the front-end (FE) electronics. The implementation of L0 is only described briefly in section 2; a fuller treatment can be found in reference [1]. The HLT consists of
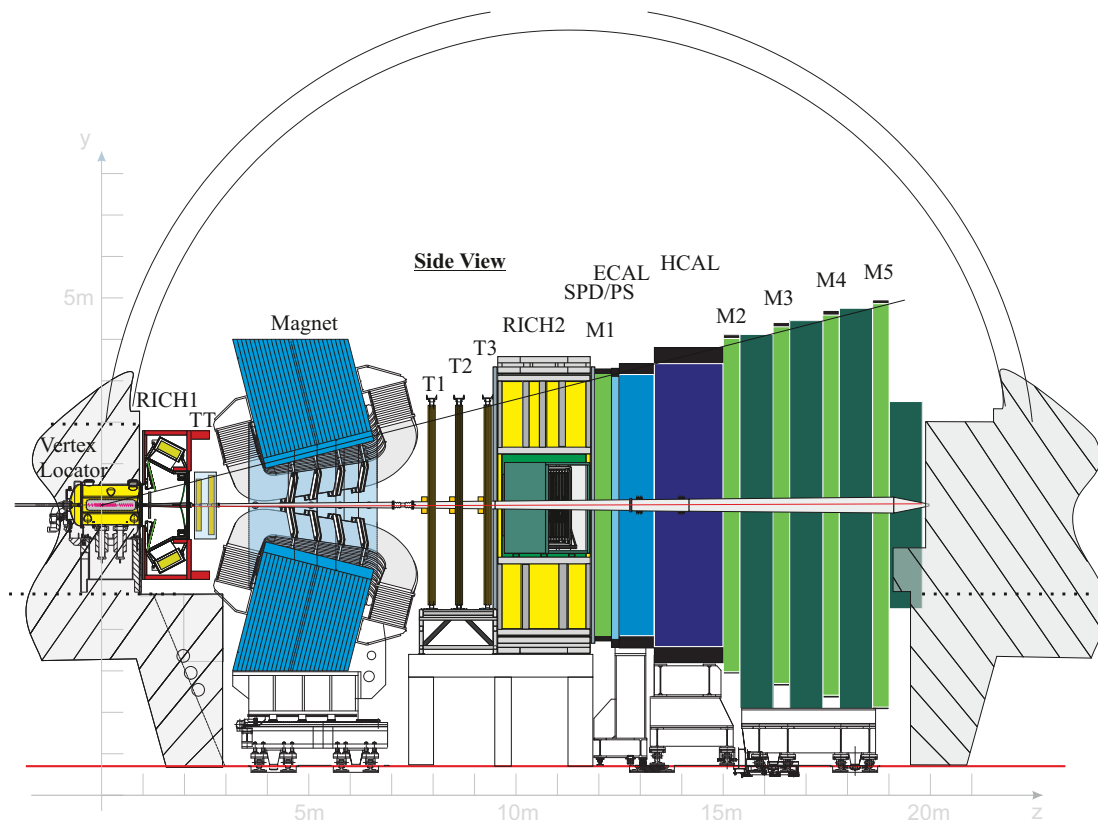
Figure 1. Layout of the LHCb detector.

a software application that runs on a farm of Personal Computers (PCs). It has evolved significantly compared to reference [1], in which it is assumed that the LHC machine would operate with a 25 ns bunch separation [2], and that LHCb would limit the number of visible pp interactions[1] such that the average number of visible interactions per bunch crossing $\mu \simeq 0.4$. However, the smallest bunch separation of the machine was 50 ns in the 2011 physics runs. To compensate for the loss in number of bunches, and combined with the fact that the LHCb detector performance did not degrade up to $\mu \approx 2.5$, LHCb decided to run at $\mu \approx 1.4$. Therefore the HLT had to adapt to running conditions rather different from those described in reference [1].

The HLT is described in detail in section 3. The HLT reduces the rate of accepted events to ~ 3 kHz, and all such events are written to storage. The events written to storage are processed with a more accurate alignment and calibration of the sub-detectors, and with reconstruction software that is more elaborate and allows for more redundancy than is possible in the HLT. This part of the reconstruction and subsequent event selection will henceforth be referred to as the off-line reconstruction and selection.

The method used to obtain a data-driven determination of the trigger performance is described in section 4. Section 5 describes the performance of the trigger in 2011 relative to off-line reconstruction and selection. Section 6 concludes with a summary of the trigger performance.

---

[1]A visible interaction is defined as one in which at least two tracks are reconstructed in the VELO, that both point to the interaction envelope.

2 First level trigger

L0 is divided into three independent triggers; the L0-Calorimeter trigger, the L0-Muon trigger and the L0-PileUp trigger. The last of these is not used to select flavour physics events, but instead aids the determination of the luminosity [5], and will not be further described in this paper.

The L0 system is fully synchronous with the 40 MHz bunch crossing signal of the LHC. The latencies are fixed and depend neither on the occupancy nor on the bunch crossing history. All of the L0 electronics are implemented in custom-designed hardware that makes use of parallelism and pipelining to do the necessary calculations within the maximum latency of $4\,\mu$s. The trigger decisions are combined in a single L0 decision, which is transferred to the Readout Supervisor board (RS). The RS generates in addition a small rate of random (NoBias) triggers taking into account the bunch filling scheme of the machine.[2] The RS emulates the state of the FE buffers to protect against their overflow. It also has information on the state of the buffers in the readout boards of all sub-detectors and the availability of the PCs in the farm. Based on this information it can retain or throttle a bunch crossing.

2.1 L0-Calorimeter trigger implementation

The L0-Calorimeter system uses information from the SPD, PS, ECAL and HCAL. These four detectors are stacked along the beam axis (z-axis) and their longitudinal segmentation offers the possibility to distinguish between photon, electron and hadron showers. Transverse to the beam axis (x-y plane) the detectors are segmented into square cells. SPD, PS and ECAL are divided into three zones with ECAL cell rib sizes of 40.4 mm in the inner zone close to the beam pipe, 60.6 mm and 121.2 mm further out. HCAL is divided into two zones with rib size 131.3 mm and 262.6 mm. The SPD, PS and ECAL have the same geometry and are projective, i.e. the sizes of the cells in the SPD and PS are adjusted to take into account the different z positions of the detectors. The HCAL cells are larger but their boundaries always correspond to the boundaries of the ECAL cells. The L0-Calorimeter system computes the transverse energy deposited in clusters of 2×2 cells, using only cells located in the same zone. Hence the cluster energy of showers with energy deposits in two adjacent zones will be too low. The transverse energy of a cluster is defined as:

$$E_T = \sum_{i=1}^{4} E_i \sin \theta_i, \tag{2.1}$$

where E_i is the energy deposited in cell i and θ_i is the angle between the z-axis and a neutral particle assumed to be coming from the mean position of the interaction envelope hitting the centre of the cell. The ECAL and HCAL signals are read out and processed in FE boards (FEB) that cover an area of $(8+1) \times (4+1)$ cells, such that the $(+1)$ cells are shared between neighbouring FEB. Each FEB selects the highest E_T cluster among its 32 clusters. From these clusters, three types of candidates are built combining information as follows:

1. Hadron candidate (`L0Hadron`): the highest E_T HCAL cluster. If there is a highest E_T ECAL cluster located in front of the HCAL cluster, the E_T of the hadron candidate is the sum of the E_T of the HCAL and ECAL clusters.

---

[2]Not all of the 3564 slots available for proton bunches around the machine are filled with protons. Most of the luminosity in 2011 was collected with 1296 bunches colliding in LHCb.

2. Photon candidate (`L0Photon`): the highest E_T ECAL cluster with 1 or 2 PS cells hit in front of the ECAL cluster and no hit in the SPD cells corresponding to the PS cells. In the inner zone of the ECAL, an ECAL cluster with 3 or 4 PS cells hit in front of it is also accepted as photon. The E_T of the candidate is the E_T deposited in the ECAL alone.

3. Electron candidate (`L0Electron`): same requirements as for a photon candidate, with in addition at least one SPD cell hit in front of the PS cells.

The E_T of the candidates is compared to a fixed threshold and events containing at least one candidate above threshold are retained by L0.

2.2 L0-Muon trigger implementation

The muon system contains five muon stations (M1–M5) consisting of pads in the high occupancy regions and horizontal and vertical strips elsewhere. Strips are combined to form logical pads for the muon trigger. The pad sizes are chosen to obtain projectivity towards the interaction region in the *y*-*z* plane. Each quadrant of the muon detector is connected to a L0 muon processor. There is no exchange of information between quadrants, hence muons traversing quadrant boundaries cannot be reconstructed in the trigger. Each of the four L0 muon processors tries to identify the two muon tracks with the largest and second largest momentum transverse to the *z*-axis (p_T) in their quadrant. The processors search for hits that define a straight line through the five muon stations and that points towards the interaction point in the *y*-*z* plane. In the *x*-*z* plane the search is limited to muons with $p_T \gtrsim 0.5\,\mathrm{GeV}/c$. The position of a track in the first two stations allows the determination of its p_T with a measured resolution of $\sim 25\%$ relative to off-line reconstructed muon tracks. The trigger sets a single threshold on either the largest p_T^{largest} of the eight candidates (`L0Muon`), or a threshold on $p_T^{\mathrm{largest}} \times p_T^{\mathrm{2nd\,largest}}$ (`L0DiMuon`).

3 High level trigger

The HLT runs on the Event Filter Farm (EFF) that is a farm of multiprocessor PCs. The HLT is a program written in C++, and 26110 copies of it run in the EFF. An event that is accepted by L0 is transferred by the on-line system from the FEB to the EFF and is assembled by one of the event builder programs that run on one of the cores of each multicore node. The assembled events are placed in a buffer that is accessed by the HLT programs that run on the cores of the node. A detailed description of this process can be found in reference [1] and references therein.

The HLT is based on the same software as used throughout LHCb data processing and simulation [3]. The off-line event reconstruction and selection requires about 2 s per event. During 2011 the L0 rate was about 870 kHz. Given the available resources in the EFF this limits the time per event in the HLT to ~ 30 ms. The HLT is divided into two stages. The first stage (HLT1) processes the full L0 rate and uses partial event reconstruction to reduce the rate to 43 kHz. At this rate the second stage (HLT2) performs a more complete event reconstruction.

A "trigger line" is composed of a sequence of reconstruction algorithms and selections. The trigger line returns an accept or reject decision. An event will be accepted by L0, HLT1 or HLT2 if it is accepted by at least one of its trigger lines at the relevant stage. Combinations of trigger

lines, together with a L0 configuration, form a unique trigger with its associated Trigger Configuration Key (TCK). The TCK is a 32 bit label pointing to a database that contains the parameters that configure the trigger lines. The TCK is stored for every event in the raw data, together with information on which trigger lines accepted the event. During 2011 running, the HLT contained 38 HLT1 and 131 HLT2 lines. The trigger lines that cover the main physics goals of LHCb [4], and accept the majority of events stored, are described below in addition to the common reconstruction algorithms. The corresponding selection parameters and their performance are given in section 5.

The remaining trigger lines consist of lines for luminosity measurements, pre-scaled physics trigger lines with looser cuts, lines that select very low multiplicity events and lines that identify large transverse momentum jets. The trigger also contains lines designed to accept NoBias events, lines that monitor events with inconsistent raw data or other errors during the HLT processing, lines that allow the VELO to monitor the position of the pp interaction envelope and lines selecting calibration and monitoring data for fast feedback on the quality of the data.

3.1 HLT1

The off-line VELO reconstruction software is fast enough to permit the full 3D pattern recognition of all events that enter the HLT. In the off-line VELO pattern recognition a second pass is made on unused hits to enhance the efficiency for tracks that point far away from the beam-line, but in the HLT this search is not executed. At the start of each LHC fill, the mean position of the pp interaction envelope in the x-y plane, PV_{xy}^{mean}, is determined using VELO tracks. This position is measured to be stable to within a few μm per fill. The VELO tracks are used to construct vertices with at least 5 tracks originating from them, and those vertices within a radius of $300\,\mu$m of PV_{xy}^{mean} are considered to be primary vertices (PV).

While in the off-line pattern recognition all VELO tracks are considered to identify the corresponding hits in the tracking stations downstream of the magnet, the pattern recognition in HLT1 limits the execution time by selecting VELO tracks that have a larger probability to originate from signal decays. HLT1 lines that do not require muons select VELO tracks based on their smallest impact parameter (IP) to any PV. In addition, cuts are applied to the quality of each VELO track based on the number of hits on a track and the expected number of hits.

For events triggered by L0Muon or L0DiMuon, a fast muon identification is performed in HLT1 to select VELO tracks that are muon candidates using the following procedure. For every VELO track, a search window is defined in the M3 station by extrapolating the VELO track in a straight line. The magnet does not bend tracks in the vertical plane, and multiple scattering dominates the vertical size of the search window. A muon candidate is required to have a momentum of at least $6\,\text{GeV}/c$, hence the horizontal search window size corresponds to the deflection of a $6\,\text{GeV}/c$ track. Hits found inside the search window are combined with the VELO track to form candidate tracks that are used in a search for additional muon hits in stations M2, M4 and M5. A candidate track is provisionally accepted if it contains at least one hit in addition to the M3 hit. In the final step of the algorithm, a linear χ^2 fit of the candidate track (containing both the VELO track and the muon hits) in the horizontal plane is performed and the χ^2 divided by the number of degrees of freedom (ndf) is required to be less than 25. As soon as the first candidate is found, the algorithm stops and the VELO track is tagged as a muon candidate.

For the VELO tracks that are selected by either their IP or by being tagged as a muon candidate, the track-segments in the OT and IT-stations are reconstructed to determine their momentum in a procedure known as forward tracking. Imposing a minimum momentum and transverse momentum (p, p_T) in the forward tracking significantly reduces the search windows that have to be opened in the IT and OT tracking stations thereby reducing the required processing time. Each reconstructed track is fitted using a Kalman filter [6] based track fit to obtain its χ^2 and a full covariance matrix at the start of the track. Compared to off-line reconstruction, this fit uses a simplified material geometry description, it makes fewer iterations and consequently it performs a less sophisticated removal of outlier hits. The invariant mass resolution of $J/\psi \rightarrow \mu^+\mu^-$ determined in the HLT is measured to be 3% larger than the $14 \, \text{MeV}/c^2$ obtained off-line. This shows that the resolution of the track parameters obtained in the HLT is sufficiently close to off-line to allow selective cuts in IP, momentum and mass. For tracks that are tagged as muon candidates, the off-line muon identification algorithm [7] is applied to the tracks to improve the purity of the muon sample.

3.2 HLT2

As mentioned above, HLT1 reduces the rate from $870 \, \text{kHz}$ to $43 \, \text{kHz}$. At this rate forward tracking of all VELO tracks can be performed in HLT2. While the off-line reconstruction uses two tracking algorithms, HLT2 only employs the algorithm based on seeding the search with VELO tracks. This leads to a lower efficiency compared to off-line of 1–2% per track. To further limit the processing time only tracks with $p > 5 \, \text{GeV}/c$ and $p_T > 0.5 \, \text{GeV}/c$ are reconstructed by limiting the search windows.

Muon identification is performed using the off-line algorithm on all tracks from the forward tracking. Tracks are also associated to ECAL clusters to identify electrons.

A large share of the 3 kHz output rate of HLT2 is selected by "topological" trigger lines, which are designed to trigger on partially reconstructed b-hadron decays. The topological trigger lines in principle cover all b-hadrons with at least two charged particles in the final state and a displaced decay vertex. The efficiencies are less dependent on reconstruction inefficiencies imposed by the minimum (p, p_T) requirements and loss due to the single, non-redundant, track reconstruction mentioned above. In the following two sections the topological trigger lines are described in more detail.

While the topological trigger lines target inclusive b-hadrons, a number of dedicated "exclusive" trigger lines are also implemented in HLT2. These require all decay particles to be reconstructed in HLT2 and use narrow mass windows to reduce their rate. These exclusive trigger lines either target prompt c-hadron production, or allow triggering on hadronic b-hadron decays without the necessity to use lifetime-biasing selections to reduce the rate. These lines are described in section 3.2.3.

3.2.1 Topological trigger lines

The decisions of the topological trigger lines are based on the properties of combinations of 2, 3, or 4 "Topo-Tracks". Topo-Tracks are a subset of HLT2 tracks selected with additional requirements on their track fit quality (χ^2/ndf), IP, and muon or electron identification. N-body (i.e. an n track combination) candidates are built as follows: two Topo-Tracks are combined into a 2-body object, requiring that their distance of closest approach (DOCA) is less than 0.2 mm. A 3(4)-body object

is made by combining a 2(3)-body object and another Topo-Track with the same DOCA < 0.2 mm cut, where the DOCA is calculated between the 2(3)-body object and the additional Topo-Track. This sequence of DOCA selections enhances the efficiency of the topological trigger lines on $B \rightarrow DX$ decays. Not all of the b-hadron final state particles need to satisfy these criteria. The trigger is designed to allow for the omission of one or more final state particles when forming the trigger candidate.

If an n-body candidate only contains a subset of the daughter particles, its invariant mass (m) will be less than the mass of a b-hadron. Thus, a mass window would need to be very loose if the trigger is to be inclusive. Instead a corrected mass (m_{corr}) is used that is defined as:

$$m_{\text{corr}} = \sqrt{m^2 + |p'_{T\text{miss}}|^2} + |p'_{T\text{miss}}|, \tag{3.1}$$

where $p'_{T\text{miss}}$ is the missing momentum transverse to the direction of flight, as defined by the PV and the n-body vertex [8]. In case of multiple PVs, the PV with respect to which the n-body combination has the smallest IP is used. The quantity m_{corr} would be the minimal mass of the parent if a massless particle was omitted from the trigger candidate. Prompt c-hadrons that are erroneously combined with another track constitute a significant fraction of the n-body candidates. These candidates are rejected by requiring that all (n − 1)-body objects used by a n-body trigger line either have a mass greater than 2.5 GeV/c^2 or that they have a significant IP to all PVs.

To select a n-body candidate, cuts are applied to the following variables: $\sum |p_T|$, $p_T^{\min}$, m, m_{corr}, DOCA, IP significance (IPχ^2) and flight distance significance (FDχ^2). Using NoBias events for background and Monte Carlo (MC) simulated signal events, we find that a larger rejection power is achieved for the same signal efficiency by combining the above variables in a multivariate selection.

3.2.2 Topological multivariate lines

To combine the variables mentioned above a boosted decision tree (BDT) was chosen; this classifier has already been successfully used elsewhere [9]. All multivariate classifiers select n-dimensional regions of a multivariate space by learning from the training samples provided to them. If selected regions are small relative to the resolution of the detector, the signal could oscillate between regions resulting in, at best, a less efficient trigger or, at worst, a trigger that is very difficult to understand. To avoid this, all of the variables are mapped onto discrete variables. The application of the BDT to discrete variables is henceforth referred to as Bonsai BDT (BBDT).

The BBDT ensures that the smallest interval that can be used satisfies $\Delta x_{\min} > \delta_x$ for all x values, where $\delta_x = \text{MIN}\{|x_i - x_j| : x_i, x_j \in x_{\text{discrete}}\}$. The constraints governing the choice of x_{discrete} are then as follows: firstly δ_x should be greater than the resolution on x and be large with respect to the expected variations in x, and secondly the discretisation should reflect common b-hadron properties.

The discretisation scheme for each variable was determined by first training a BBDT with a very large number of discretisation values and then gradually decreasing this number while maintaining near optimal performance. The training signal samples were MC simulated data that contained as signal B^+, B^0, B_s or Λ_b decays[3] with decay modes as given in table 1, while the background sample was NoBias data recorded in 2010. Table 2 shows the discretisation scheme for each of the variables used in the BBDT.

---

[3]Charge conjugate hadrons are always implied.

Table 1. MC signal samples used to train the BBDT, where K means $K^\pm$ and π means $\pi^\pm$.

Parent	Daughters
B^+	$K\pi\pi,\ D_{[K\pi]}\pi,\ D_{[hhhh]}K,\ D_{[K_S\pi\pi]}K,\ D_{[K\pi\pi]}K\pi$
B^0	$K^*_{[K\pi]}\mu\mu,\ K^*_{[K\pi]}ee,\ D_{[K\pi\pi]}\pi,\ K\pi,\ D_{[K\pi]}K\pi,\ D^*_{[D(K\pi)\pi]}\mu\nu,\ D_{[K\pi\pi]}K\pi\pi$
B_s	$D_{s[KK\pi]}\pi,\ D_{s[KK\pi]}K\pi\pi,\ K^*_{[K\pi]}K^*_{[K\pi]}$
Λ_b	$\Lambda_{c[pK\pi]}\pi,\ \Lambda_{c[pK\pi]}K\pi\pi$

Table 2. Allowed mapping points in the BBDT. The variables are explained in the text.

Variable	Cuts (2, 3, 4-body)	Intervals used in the BBDT
$\sum \lvert p_T \rvert$ [GeV/c]	$> 3, 4, 4$	3.5, 4, 4.5, 5, 6, 7, 8, 9, 10, 15, 20
$p_T^{\min}$ [GeV/c]	> 0.5	0.6, 0.7, 0.8, 0.9, 1, 1.25, 1.5, 1.75, 2, 2.5, 3, 4, 5, 10
m [GeV/c^2]	< 7	2.5, 4.75
m_{corr} [GeV/c^2]		2, 3, 4, 5, 6, 7, 8, 9, 10, 15
DOCA [mm]	< 0.2	0.05, 0.1, 0.15
IPχ^2		20
FDχ^2/100	> 1	2, 3, 4, 5, 6, 7, 8, 9, 10, 25, 50, 100

3.2.3 Exclusive lines

In the topological trigger described in the previous section there is an explicit veto on prompt charm. The selection of prompt charm decays is achieved by HLT2 lines that require a reconstruction of all the decay products, and have tight cuts on the invariant mass of the reconstructed candidates. While HLT2 reconstruction and selection efficiencies for b-hadrons are good, the $p_T > 0.5\,\mathrm{GeV}/c$ constraint reduces the efficiency for the exclusive selection of charm decays with more than two final state particles. To enhance the reconstruction efficiency for these exclusive trigger lines, the trigger lines first try to identify a two-prong secondary vertex. Selection cuts are imposed on the maximum invariant mass of the two tracks, the quality of their vertex, the sum of the transverse momenta of the tracks and m_{corr}. These initial cuts reduce the rate sufficiently to allow for the forward tracking of the remaining VELO tracks, but now with a relaxed $p_T > 0.25\,\mathrm{GeV}/c$ constraint and only using the hits in the tracking system that have not been used by the previous pass in forward tracking. Two-prong candidates are subsequently combined with other tracks, which now include the low p_T tracks, to form exclusively reconstructed candidates. The combinatorial background is reduced by tight requirements on the mass and on the angle between the momentum of the D and the vector connecting the PV with the D vertex. HLT2 contains 28 trigger lines dedicated to selecting prompt charm.

Another example of an exclusive trigger is a dedicated trigger line selecting the decay $B_s \to K^+ K^-$ while avoiding cuts that bias the B_s lifetime. This implies that a cut on IP, a powerful variable to reject combinatorial background, cannot be used. In order to enrich the B_s candidates two dedicated neural networks based on the NeuroBayes neural network package [10] are used. In a first step, kinematic constraints such as the transverse momentum of the final state particles

and the helicity angle in the rest frame of the B_s candidate are used to reduce the rate. This allows running the comparatively slow particle identification algorithm using the RICH sub-detector on the events selected by the first neural network. This information is then included in a second neural network that uses both kinematic and particle ID information to make the final selection.

4   Data-driven trigger performance determination

The trigger performance is evaluated relative to offline reconstruction and selections, and thus contains only the additional inefficiency due to simplifications used in the trigger, possible alignment inaccuracies, worse resolution than the offline reconstruction or harder cuts imposed by rate and/or processing time limitations. The following channels have been chosen to show the performance of the trigger: $D^0 \to K^-\pi^+$, $D^+ \to K^-\pi^+\pi^+$, $B^+ \to J/\psi(\mu^+\mu^-)K^+$, $B^0 \to D^-(K^+\pi^-\pi^-)\pi^+$, $B^- \to D^0(K^-\pi^+)\pi^-$, $B^0 \to J/\psi(e^+e^-)K^{*0}(K^+\pi^-)$ and $B^0 \to K^{*0}(K^+\pi^-)\gamma$. These channels and their selections are representative for those used in most analyses. In all off-line selected signal samples the level of background is significantly lower than the signal. Substantial differences in trigger efficiency, however, are observed for true signal and background. The trigger performance on each channel is measured by determining the signal component using fits to the invariant mass distributions, hence avoiding any background contamination.

In what follows, the term "signal" refers to a combination of tracks that form the off-line reconstructed and selected b or c-hadron candidate. To determine the trigger efficiency, trigger objects are associated to signal tracks. The trigger records all the information needed for such an association. All strips, straws, cells and pads of the sub-detectors have a unique identifier, and these identifiers are written in a trigger report in the data stream for every trigger line that accepts an event. The criteria used to associate a trigger object with a signal track are as follows:

- L0-Calorimeter: the off-line track is extrapolated to the z-position of the calorimeter (ECAL or HCAL), and the cells intersecting with the track and its eight neighbours are considered signal cells. If any of the 2×2 cells of a L0-Calorimeter cluster above the threshold coincides with a signal cell, this cluster is associated with the off-line track. If none of the cells overlap, the cluster is not associated with the off-line track.

- L0-Muon: the trigger records the M1, M2 and M3 hits used to form the L0 muon candidate. If at least two of the three hits are shared with an off-line reconstructed muon the L0 muon is associated with the off-line track. Non-associated L0 muons have no hits overlapping between the L0 muon and the muon hits of the off-line track.

- HLT tracks: a HLT track has VELO hits and hits in the OT and/or the IT. In addition it can have TT hits and hits in the muon chambers M2–M5. Associated tracks require that the fraction of HLT track hits that overlaps with the off-line track is at least 70% in the VELO, 70% in the TT if applicable and 70% of the OT and IT combined. For muons the association requirement is that at least 60% of the HLT muon hits overlap with the off-line muon. Non-associated HLT tracks share no hits with the off-line track.

An event is classified as TOS (Trigger on Signal) if the trigger objects that are associated with the signal are sufficient to trigger the event. An event is classified as TIS (Trigger Independent of
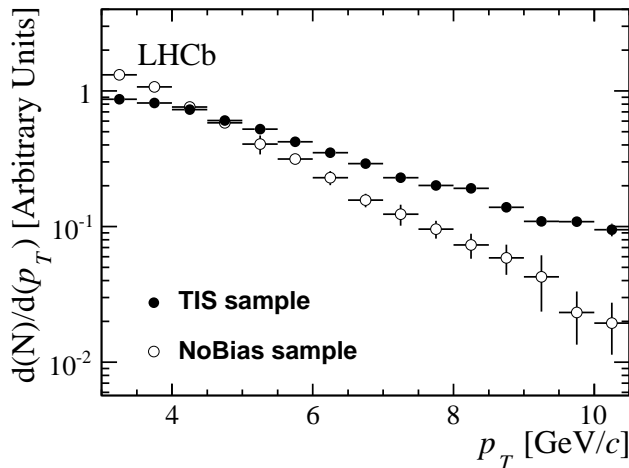
Figure 2. Comparison of the p_T distributions of $D^+ \rightarrow K^-\pi^+\pi^+$ selected in NoBias and TIS events.

Signal) if it could have been triggered by those trigger objects that are not associated to the signal. Global event variables, such as the number of primary vertices or the SPD multiplicity, are not considered in this classification. A number of events can be classified as TIS and TOS simultaneously ($N^{\text{TIS\&TOS}}$), which allows the extraction of the trigger efficiency relative to the off-line reconstructed events from data alone. The efficiency to trigger an event independently of the signal, ε^{TIS}, is given by $\varepsilon^{\text{TIS}} = N^{\text{TIS\&TOS}}/N^{\text{TOS}}$, where N^{TOS} is the number of events classified as TOS. The efficiency to trigger an event on the signal alone, ε^{TOS}, is given by $\varepsilon^{\text{TOS}} = N^{\text{TIS\&TOS}}/N^{\text{TIS}}$, where N^{TIS} is the number of events classified as TIS. The total trigger efficiency for events containing the signal can then be computed as $\varepsilon^{\text{TIS}} \times N^{\text{Trig}}/N^{\text{TIS}}$, where N^{Trig} is the total number of triggered signal events.

The phase-space distribution of the signal is affected by the TIS requirement. This is illustrated in figure 2, which shows the p_T distribution of $D^+ \rightarrow K^-\pi^+\pi^+$ candidates selected from NoBias and TIS events. The p_T of TIS events is harder, which would result in a too large signal efficiency when integrated over all phase-space. This bias in phase-space can be understood considering that $c\bar{c}$, or $b\bar{b}$, pairs are correlated in phase-space at production, and TIS events are predominantly triggered by the decay products of the hadron that contains the other heavy quark. Another example of bias is that for charm decays TIS events could enhance the non prompt charm component by triggering on the other decay products of a B to D decay. These biases can only be evaluated individually for each analysis. Therefore the trigger performance is presented as a function of the signal p_T and its lifetime (τ).

5 Trigger performance

For each channel ε^{TOS} is determined relative to the off-line selection efficiency of a channel. ε^{TOS} for the HLT1(2) performance is given for off-line selected events that have also been classified as TOS in the previous trigger level(s), unless mentioned otherwise.

At each trigger level the different trigger lines compete for their share of the available resources. To determine the different selections for the trigger lines, a "bandwidth division" proce-

dure has been adopted, which is described in the next section. The performance of the different trigger lines with the thresholds as determined by the bandwidth division will be presented for L0, HLT1 and HLT2 in the next sections for the channels listed in section 4.

5.1 Bandwidth division procedure

The bandwidth division minimises the overall loss in efficiency by minimising the following:

$$\sum_{\text{signal}} \left(\sum_{\text{lines}} \left(1 - \frac{\varepsilon^{\text{signal, line}}}{\varepsilon_{\text{max}}^{\text{signal, line}}} \right) \right)^2, \tag{5.1}$$

where $\varepsilon^{\text{signal, line}}$ is the L0 × HLT trigger efficiency obtained using a set of selections (corresponding to a single set of cut values) for all signal channels and trigger lines simultaneously and $\varepsilon_{\text{max}}^{\text{signal, line}}$ is the maximum of $\varepsilon^{\text{signal, line}}$ with the full computing resources dedicated to that signal and specific trigger line alone. The score is evaluated for each set of cuts by running an emulation of the L0 trigger and executing the HLT application. This emulation includes FE-buffer overflow emulation, the available processing power in the EFF and the maximal HLT2 output rate to disk as boundary conditions. The configuration with the minimum score is found by varying the cuts and running the trigger software for each variant.

For signal the following MC generated and off-line reconstructed and selected channels have been chosen to represent both the main physics goals of LHCb and to cover all the trigger components that need to be tuned: $B_s \to J/\psi(\mu^+\mu^-)\phi(K^+K^-)$, $B_s \to \mu^+\mu^-$, $B^0 \to K^{*0}\mu^+\mu^-$, $B_{(s,d)} \to \mu^+X$, $D^{*+} \to D(\mu^+\mu^-)\pi^+$, $D^+ \to K^-\pi^+\pi^+$, $B^0 \to K^{*0}\gamma$, $B^0 \to K^+\pi^-$, $B^0 \to K^{*0}e^-e^+$, $B^+ \to K^+\pi^-\pi^+$, $B_s \to D_s^-(K^+K^-\pi^-)K^+$, $B^+ \to \bar{D}^0(K_S(\pi^+\pi^-)\pi^+\pi^-)K^+$ and $D^0 \to K^-\pi^+$ with $K^{*0} \to K^+\pi^-$. NoBias events from 2010 with $\mu = 1.4$ are used as background. Rather than introducing weights favouring some channels, we have chosen to emphasize the main physics goals by the number of channels included in the bandwidth division procedure. For example, channels decaying with muons in the final state are more abundant.

All performance results are given for 1296 colliding bunches in LHCb, which corresponds to a bunch crossing rate with at least one visible pp interaction of $\sim 11\,\text{MHz}$. The bandwidth division yields the following rates for NoBias events: 870 kHz for L0, 43 kHz for HLT1 and 3 kHz for HLT2.

5.2 L0 performance

Events with a large occupancy in the OT and IT consume a disproportionately large fraction of the available processing time in the HLT. The SPD multiplicity measured at L0 is a good measure of this occupancy, permitting an early rejection of events that require a relatively large processing time. Using the bandwidth division the optimal SPD cut is determined to be < 900 for events triggered by `L0DiMuon` and < 600 for all other L0 triggers. On average, events with a SPD multiplicity larger than 600 consume four times more time in the HLT than events with less than 600 SPD hits. The fraction of events rejected due to these cuts has been determined from real data for charm hadron production to be $7.4 \pm 0.3\,(0.05 \pm 0.01)\%$ for a cut on $600\,(900)$ in SPD multiplicity. Similarly for b-hadron production the fraction of events with a SPD multiplicity $> 600\,(900)$ is

Table 3. Cuts of L0 lines and their rates prior to throttling. The definition of the trigger lines is given in section 2.

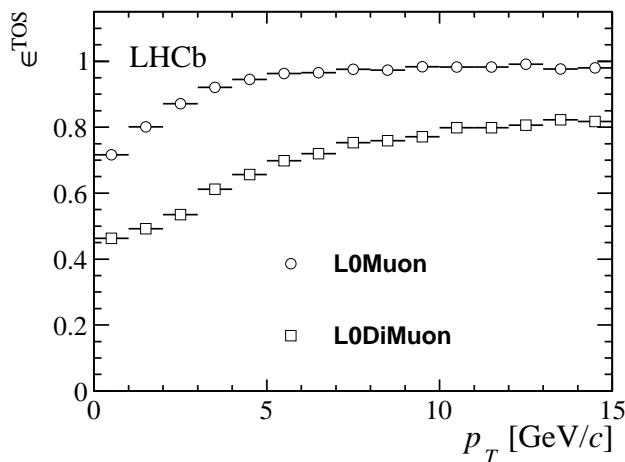|	Threshold	SPD Multiplicity	Rate
L0Muon	$p_T > 1.48\,\text{GeV}/c$	< 600	340 kHz
L0DiMuon	$\sqrt{p_T{}^{\text{largest}} \times p_T{}^{\text{2nd largest}}} > 1.296\,\text{GeV}/c$	< 900	75 kHz
L0Hadron	$E_T > 3.5\,\text{GeV}$	< 600	405 kHz
L0Electron	$E_T > 2.5\,\text{GeV}$	< 600	160 kHz
L0Photon	$E_T > 2.5\,\text{GeV}$	< 600	80 kHz

Figure 3. Efficiency ε^{TOS} of $B^+ \to J/\psi\,(\mu^+\mu^-)K^+$ as a function of p_T (J/ψ) for L0Muon and L0DiMuon lines.

found to be $8.8 \pm 0.6\,(0.5 \pm 0.2)\%$. All efficiencies quoted below are given relative to the sample after the SPD multiplicity cut.

Table 3 lists the L0 cuts. About 20% of the events accepted by L0 are selected by more than one trigger line, giving a total L0 rate of 870 kHz prior to throttling. L0Muon is the main trigger for particle decays with one or more muons in the final state. L0DiMuon recovers part of the events with a SPD multiplicity > 600 for a small increase in rate. The performance of L0Muon and L0DiMuon are shown in figure 3 for $B^+ \to J/\psi\,(\mu^+\mu^-)K^+$ as a function of p_T (J/ψ). L0DiMuon increases the number of signal events by 4.9%, of which 87% have a SPD multiplicity larger than 600 hits. The remaining 13% is due to the lower p_T cut in L0DiMuon. L0 requires a muon candidate to have a hit in all five muon stations, while off-line as few as two stations are sufficient to identify a muon. As a result L0DiMuon has a maximum efficiency of $\sim 80\%$ even for a J/ψ with large p_T. L0Muon recovers this loss for lower SPD multiplicities and decays with more muons at large p_T.

L0Hadron selects heavy flavour decays with hadrons in the final state. The performance of L0Hadron is shown in figure 4 for $B^0 \to D^- \pi^+$, $B^- \to D^0 \pi^-$, $D^0 \to K^- \pi^+$ and $D^+ \to K^- \pi^+ \pi^+$ as a function of p_T of the signal B and D mesons. At low p_T, L0Hadron has a better efficiency for b-hadrons than for c-hadrons due to the larger b-hadron mass. Once the p_T of the hadron is above the b-hadron mass, the decays with fewer final state tracks have a higher efficiency.
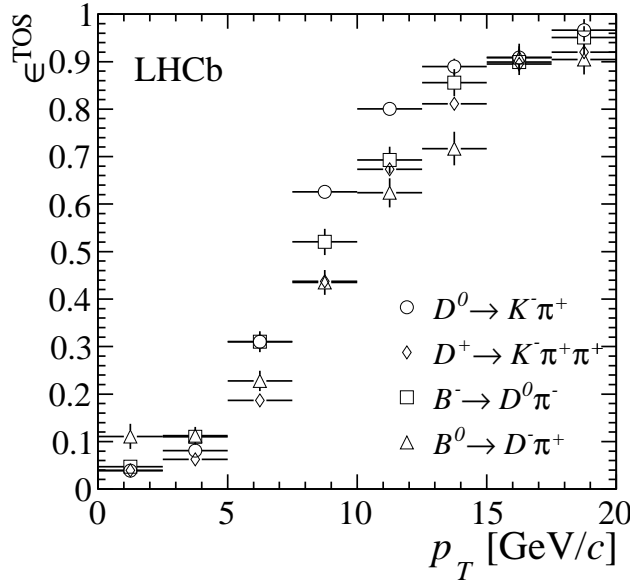
Figure 4. The efficiency ε^{TOS} of L0Hadron is shown for $B^0 \to D^- \pi^+$, $B^- \to D^0 \pi^-$, $D^0 \to K^- \pi^+$ and $D^+ \to K^- \pi^+ \pi^+$ as a function of p_T of the signal B and D mesons.
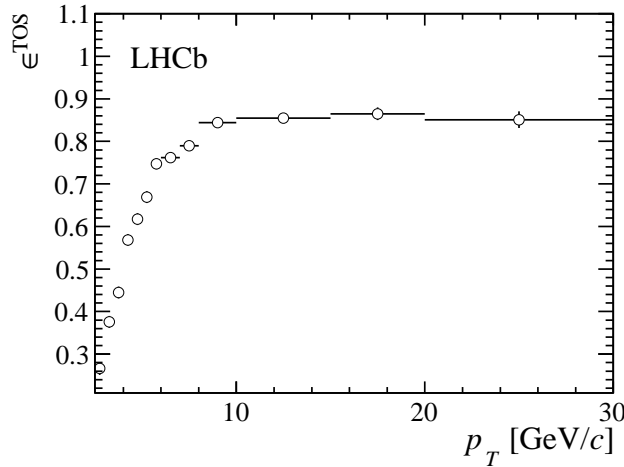

Figure 5. The efficiency ε^{TOS} of L0Electron is shown for $B^0 \to J/\psi(e^+e^-)K^{*0}$ as a function of p_T (J/ψ).

L0Electron selects decays with electrons in the final state. It also triggers on radiative decays, with the photon being either converted, or with photon clusters with SPD hits in front due to overlapping charged particles. The performance of L0Electron is shown in figure 5 for $B^0 \to J/\psi(e^+e^-)K^{*0}$ as a function of $p_T(J/\psi)$. Contrary to L0Muon, L0Electron is not fully efficient for J/ψ with large p_T. This is due to the hardware implementation (see section 2.1) that prevents energy deposited in different ECAL zones from being combined into one cluster.

The performance of the trigger for high-energy photons from radiative penguin decays is measured with the channel $B^0 \to K^{*0}\gamma$. The number of TIS events in this channel is insufficient to study the efficiency as a function of p_T of the B^0. The mean efficiency for the L0Photon line integrated

Table 4. HLT1 muon lines and their cuts. The rate is measured on events accepted by LOMuon or LODiMuon.

Hlt1line	TrackMuon	SingleMuon HighPT	DiMuon HighMass	DiMuon LowMass
Track IP [mm]	> 0.1	–	–	–
Track IPχ^2	> 16	–	–	> 3
Track p_T [GeV/c]	> 1	> 4.8	> 0.5	> 0.5
Track p [GeV/c]	> 8	> 8	> 6	> 6
Track χ^2/ndf	< 2	< 4	< 4	< 4
DOCA [mm]	–	–	< 0.2	< 0.2
χ^2_{vertex}	–	–	< 25	< 25
Mass [GeV/c^2]	–	–	> 2.7	> 1
Rate [kHz]	5	0.7	1.2	1.3

over p_T is $50 \pm 4\%$. Selecting events with either LOPhoton or LOElectron gives an efficiency of $88 \pm 5\%$.

5.3 HLT1 performance

HLT1 muon lines are only executed for events that have been triggered by LOMuon or LODiMuon, and the lines require their tracks to be validated as a muon candidate as described in section 3.1. Table 4 gives the names of the HLT1 muon lines and their cuts. Hlt1TrackMuon accepts events with B, D or τ decays with at least one muon in its final state by identifying and accepting events with muon candidates that have significant IP with respect to all PVs. To trigger on muons originating from heavy particles with a negligible lifetime, like $W^\pm$ or Z^0, an alternative line, Hlt1SingleMuonHighPT, is implemented. It does not have any requirements on IP, but requires a hard p_T cut to reduce the rate. Hlt1DiMuonHighMass is complementary to Hlt1TrackMuon in that it allows b-hadron decays to be selected without imposing lifetime related cuts, and thus allows the lifetime acceptance bias of the larger efficiency Hlt1TrackMuon line to be determined. Finally Hlt1DiMuonLowMass allows triggering on final states with two muons with a relatively small invariant mass. To reduce the rate the line requires that both muons are not prompt.

The performance of the HLT1 muon lines is evaluated using $B^+ \rightarrow J/\psi K^+$ decays. Figure 6 shows the performance of Hlt1TrackMuon, Hlt1DiMuonHighMass and Hlt1DiMuonLowMass as a function of the p_T and τ of the B^+. Hlt1TrackMuon gives the best performance overall, except at low lifetimes, where Hlt1DiMuonHighMass recovers events. Hlt1DiMuonLowMass loses $\sim 10\%$ in efficiency compared to Hlt1TrackMuon for $B^+ \rightarrow J/\psi K^+$ due to the requirement to have at least two muon candidates, but its cuts on IP and p_T are significantly relaxed to allow the selection of candidates with the muon pair mass down to $1 \, \mathrm{GeV}/c^2$, which is designed to select $b \rightarrow s\mu\mu$ decays like $B \rightarrow K^* \mu^+ \mu^-$.

The performance of Hlt1SingleMuonHighPT is not properly assessed using $B^+ \rightarrow J/\psi K^+$ decays because it is designed to accept events with decays of particles with a mass larger than that of b-hadrons. Instead $Z^0 \rightarrow \mu^+ \mu^-$ events are used to measure the efficiency, by requiring one of the
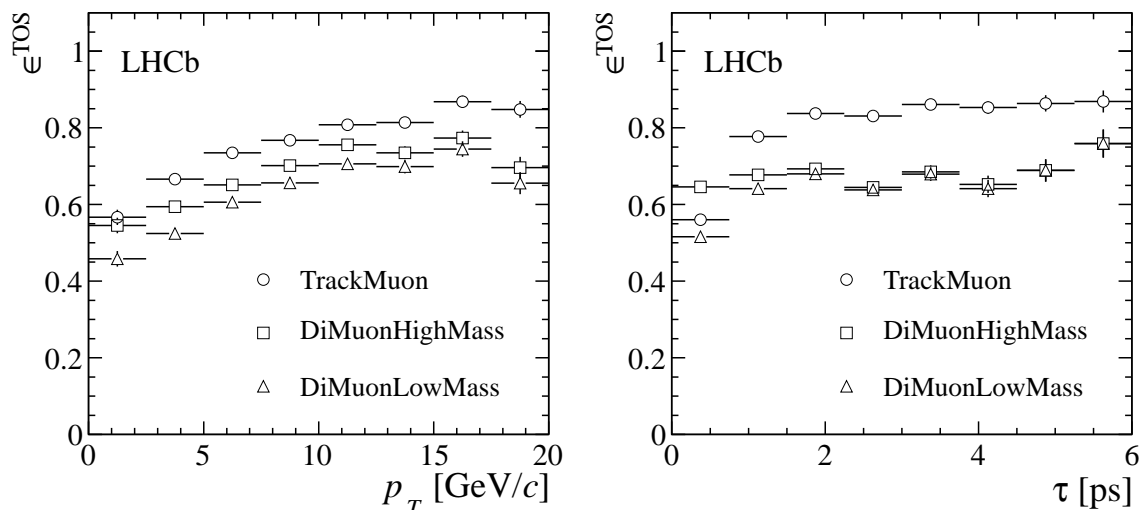
Figure 6. Efficiency ε^{TOS} of `Hlt1TrackMuon`, `Hlt1DiMuonHighMass` and `Hlt1DiMuonLowMass` for $B^+ \rightarrow J/\psi(\mu^+\mu^-)K^+$ as a function of the p_T and lifetime of the B^+.

two muons to be TIS. This yields an efficiency of $77.1 \pm 0.2\%$ for the `Hlt1SingleMuonHighPT` line per single muon, implying an efficiency for $Z^0 \rightarrow \mu^+\mu^-$ of 95%. The fast HLT1 muon reconstruction, as described in section 3.1, applies more stringent cuts than the off-line muon identification to keep misidentification and as a consequence the rate and CPU time consumption under control.

In addition to the muon lines mentioned above, HLT1 also contains a line that is executed for all events accepted by L0, `Hlt1TrackAllL0`. It is designed to select hadron decays which are significantly displaced from a PV. A trigger line called `Hlt1TrackPhoton` is only executed for events that have a `L0Photon` or a `L0Electron` with $E_T > 4.2\,\text{GeV}$. This trigger line is designed to enhance the trigger efficiency for radiative b-hadron decays with a high p_T photon. The corresponding selection cuts are given in table 5. Both trigger lines require at least one track with sufficient IP and p_T. `Hlt1TrackPhoton` is designed to select lower p_T tracks, and correspondingly also has relaxed track quality requirements compared to `Hlt1TrackAllL0`. Figure 7 shows the performance of `Hlt1TrackAllL0` as a function of p_T and τ for channels with hadronic decays. `Hlt1TrackAllL0` provides a very efficient trigger for all heavy flavour decays with a significant flight distance from their PV, reducing the rate from 870 kHz to 33 kHz. At low p_T the requirement of at least one decay particle with $p_T > 1.7\,\text{GeV}/c$ results in selecting b-hadrons with a larger efficiency than c-hadrons, and low multiplicity decays with a larger efficiency than higher multiplicity decays. At large p_T this condition favours the decays with larger multiplicities. While in L0 special lines are used to select b-hadron decays with electrons in the final state, in HLT1 these decays are covered by `Hlt1TrackAllL0`.

There are insufficient radiative B-decays to extract the performance of `Hlt1TrackPhoton` as a function of p_T in a data-driven way. `Hlt1TrackPhoton` uses the same tracks as `Hlt1TrackAllL0`, but with a relaxed set of requirements as shown in table 5. The yield increase in $B^0 \rightarrow K^{*0}\gamma$ events obtained by including `Hlt1TrackPhoton` in addition to `Hlt1TrackAllL0` is measured to be $12 \pm 2\%$.

Table 5. The cuts applied in `Hlt1TrackAllL0` and `Hlt1TrackPhoton` lines. The rate is measured on events accepted by L0.

Hlt1 line	Hlt1TrackAllL0	Hlt1TrackPhoton
Track IP [mm]	> 0.1	> 0.1
Number VELO hits/track	> 9	> 6
Number missed VELO hits/track	< 3	< 3
Number OT+IT $\times$ 2 hits/track	> 16	> 15
Track IPχ^2	> 16	> 16
Track p_T [GeV/c]	> 1.7	> 1.2
Track p [GeV/c]	> 10	> 6
Track χ^2/ndf	< 2.5	< 2.5
Rate [kHz]	33	4.2
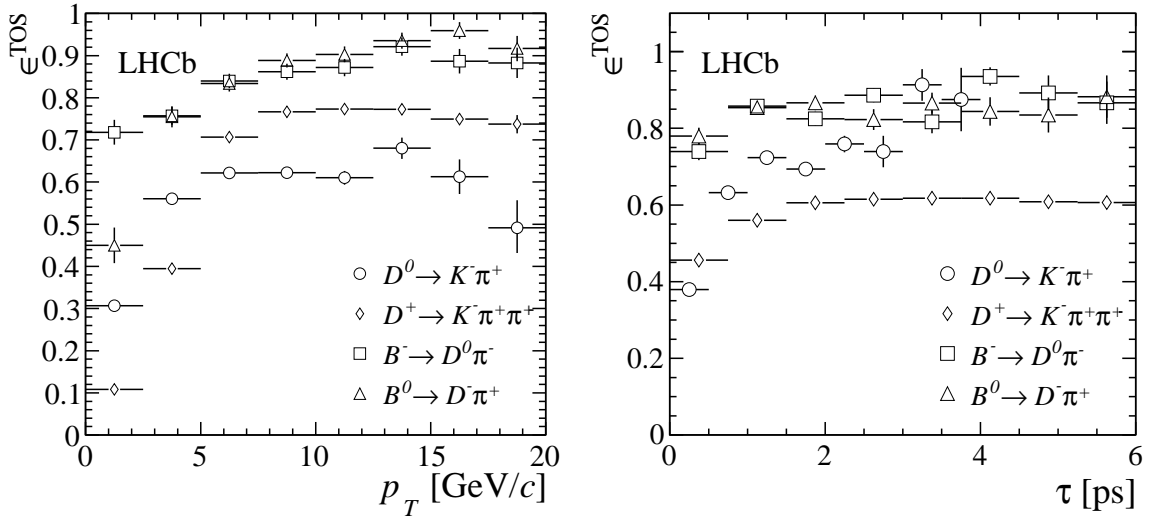
Figure 7. Efficiency $\varepsilon^{\mathrm{TOS}}$ of `Hlt1TrackAllL0` is shown for $B^- \to D^0\pi^-$, $B^0 \to D^-\pi^+$, $D^0 \to K^-\pi^+$ and $D^+ \to K^-\pi^+\pi^+$ as a function of p_T and τ of the B-meson and prompt D-meson respectively.

5.4 HLT2 performance

Similar to HLT1, HLT2 has lines that select events with one or two identified muons in the final state. In HLT2 the muon identification is identical to the off-line algorithm. The cuts corresponding to lines that are purely based on a single identified muon are given in table 6. `Hlt2SingleMuon` selects semileptonic b and c-hadron decays. To minimise the bias on the hadronic part of the decay the p_T cut is set low, in combination with scaling the rate down by a factor two, rather than tightening the cut to reduce the rate. This trigger line also provides a large yield for $J/\psi \to \mu\mu$ events that are selected by one of the two muons, while the other muon is used for calibration of tracking and muon identification efficiencies. `Hlt2SingleMuonHighPT` is designed to select heavy particles decaying promptly to one or more muons, like $W^\pm$ or Z^0. Contrary to `Hlt2SingleMuon` the rate is not a problem so there is no HLT1 requirement imposed. As for HLT1, $Z^0 \to \mu^+\mu^-$

Table 6. HLT2 lines based on one identified muon.

Hlt2Single	Muon	MuonHighPT
Hlt1TrackMuon	TOS	−
Track IP [mm]	> 0.5	−
Track IPχ^2	> 200	−
Track p_T [GeV/c]	> 1.3	> 10
Track χ^2/ndf	< 2	−
Pre-scale	0.5	1.
Rate [Hz]	480	45

Table 7. HLT2 lines based on two identified muon.

Hlt2DiMuon	JPsi	Psi2S	B	JPsiHighPT	Psi2SHighPT
Track χ^2/ndf	< 5	< 5	< 5	< 5	< 5
Mass [GeV/c^2]	$M_{J/\psi} \pm 0.12$	$M_{\psi(2S)} \pm 0.12$	> 4.7	$M_{J/\psi} \pm 0.12$	$M_{\psi(2S)} \pm 0.12$
χ^2_{vertex}	< 25	< 25	< 10	< 25	< 25
$p_T{}^{\mu\mu}$ [GeV/c]	−	−	−	> 2	> 3.5
Pre-scale	0.2	0.1	1.	1.	1.
Rate [Hz]	50	5	80	115	15

decays are used to measure an efficiency of over 99% for Hlt2SingleMuonHighPT per muon. This small loss in efficiency is attributed to different alignment constants and the non-redundant track reconstruction used in HLT2 as described in section 3.2.

The HLT2 lines that are based on two identified muons are grouped into two categories. Those that are dedicated to prompt decays use the mass as the main discriminant, while "detached" lines use the separation between the dimuon vertex and the PV as the main discriminant. The names and corresponding cuts of the prompt decay selections are given in table 7. Hlt2DiMuonJPsi(Psi2S) and Hlt2DiMuonJPsi(Psi2S)HighPT all select a mass region around J/ψ ($\psi(2S)$). Hlt2DiMuonJPsi(Psi2S) avoids explicit p_T requirements but as a consequence needs to be pre-scaled to reduce the rate. Hlt2DiMuonJPsi(Psi2S)HighPT reduces the prompt J/ψ ($\psi(2S)$) rate by applying a p_T cut on the J/ψ ($\psi(2S)$) candidate. Hlt2DiMuonB has its mass cut set high enough to have an acceptable rate.

The names and corresponding cuts of the detached decay selections are given in table 8. Hlt2DiMuonDetached is the main trigger for low mass muon pairs. Hlt2DiMuonDetachedHeavy is an analogous trigger line for J/ψ and higher mass muon pairs, with relaxed lifetime selection criteria. Hlt2DiMuonDetachedJPsi enhances the efficiency for J/ψ by reducing the flight distance requirement for J/ψ candidates even further. Figure 8 compares the performance of two representative HLT2DiMuon lines: Hlt2DiMuonJPsiHighPT and Hlt2DiMuonDetachedJPsi in $B^+ \to J/\psi K^+$ decays. Hlt2DiMuonJPsiHighPT avoids by design a bias in the proper lifetime, at the price of losing efficiency at low $p_T(J/\psi)$. The detached lines allow the selection of decays with

Table 8. HLT2 lines based on two identified muons.

Hlt2DiMuon	Detached	DetachedHeavy	DetachedJPsi
Track χ^2/ndf	< 5	< 5	< 5
Track IPχ^2	> 9	$-$	$-$
Mass [GeV/c^2]	> 1	> 2.95	$M_{J/\psi} \pm 0.12$
FDχ^2	> 49	> 25	> 9
χ^2_{vertex}	< 25	< 25	< 25
$p_T{}^{\mu\mu}$ [GeV/c]	> 1.5	$-$	$-$
Rate [Hz]	70	75	35
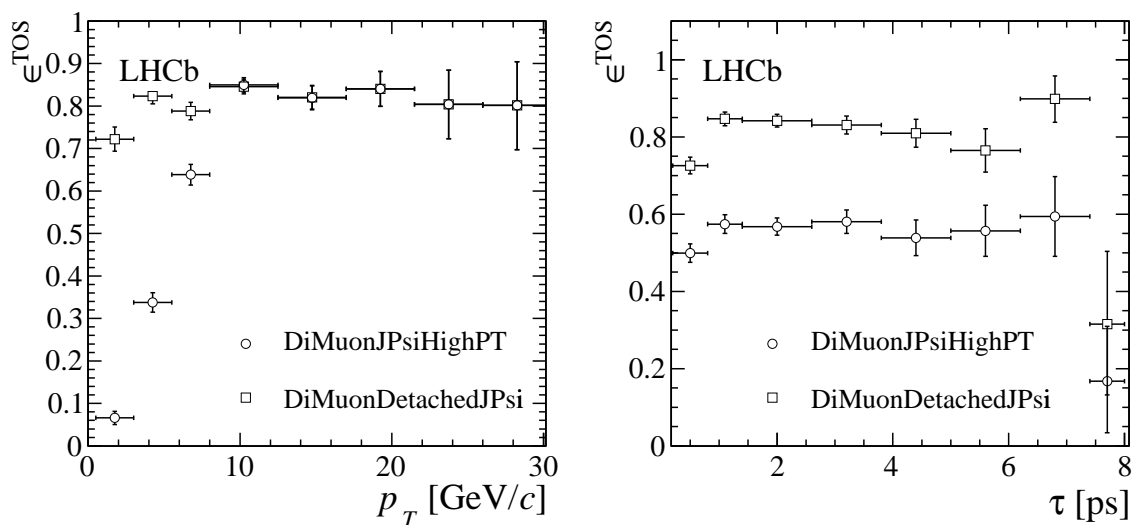
Figure 8. Efficiencies ε^{TOS} of Hlt2DiMuonJPsiHighPT and Hlt2DiMuonDetachedJPsi for $B^+ \to J/\psi K^+$ as a function of p_T and τ of the B^+.

a significant flight distance with high efficiency even at low $p_T(J/\psi)$, but their efficiency is reduced at small lifetimes.

There are nine BBDT topological lines: Hlt2Topo$n$Body, Hlt2TopoMunBody and Hlt2TopoEnBody, where $n = 2, 3, 4$ for the multiplicities considered. TopoMu (TopoE) require at least one of the decay particles to have been identified as a muon (electron). Each line returns an output of the BBDT between 0 and 1. Hlt2Topo$n$Body lines accept events with a combined rate of 930 Hz with a cut on the BBDT output at 0.4, 0.4 and 0.3 for the 2, 3 and 4 body lines respectively. While the TopoMu and TopoE lines are based on the same BBDT, the extra requirement of either a muon or electron allows the cut on the BBDT output to be reduced to 0.1 for all six lines, which results in rates of 290 and 260 Hz for TopoMu and TopoE respectively.

The performance of the topological lines is given in figure 9 for fully hadronic B-decays and figure 10 for $B^+ \to J/\psi K^+$ decays. Figure 10 also shows the complementarity of Hlt2Topo$n$Body and Hlt2TopoMunBody; the efficiency increases if either of these lines has selected the signal event. The inclusive performance of the topological lines is demonstrated in figure 10 by giving
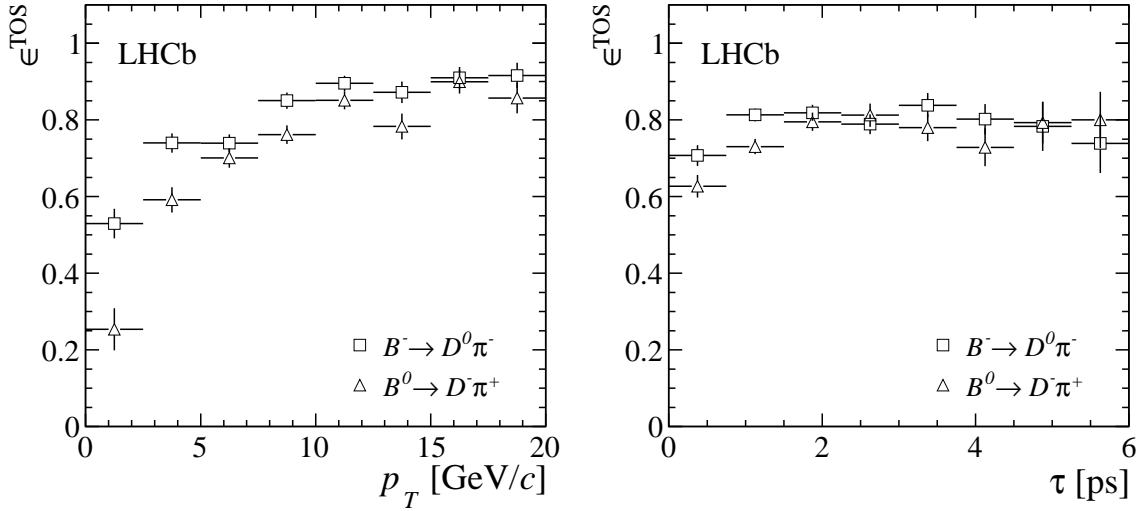
Figure 9. Efficiency $\varepsilon^{\mathrm{TOS}}$ if at least one of the lines Hlt2Topo$n$Body, with $n = 2, 3$, selected the event for $B^- \to D^0 \pi^-$ and one of the lines with $n = 2, 3, 4$ for $B^0 \to D^- \pi^+$ as a function of p_T and τ of the B-meson. The efficiency is measured relative to events that are TOS in Hlt1TrackAllL0.
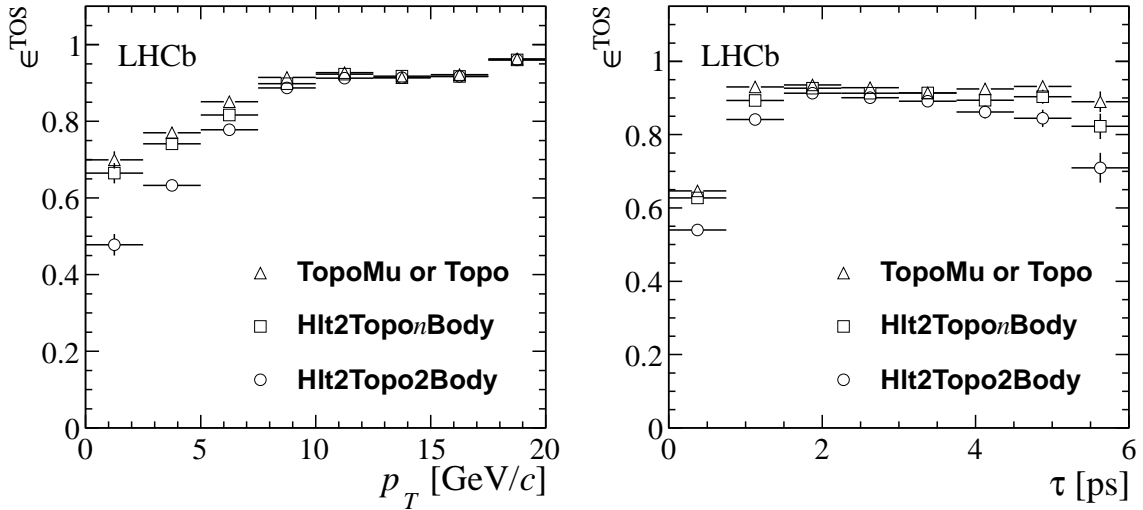

Figure 10. Efficiency $\varepsilon^{\mathrm{TOS}}$ if at least one of the lines Hlt2Topo$n$Body or Hlt2TopoMunBody, with $n = 2, 3$, selected events for $B^+ \to J/\psi K^+$, as a function of p_T and τ of the B-meson. Also shown is $\varepsilon^{\mathrm{TOS}}$ if the line Hlt2Topo$n$Body, with $n = 2, 3$, selected the events. Hlt2Topo2Body shows the inclusive performance of the topological lines. The efficiency is measured relative to events that are TOS in either Hlt1TrackAllL0 or Hlt1TrackMuon.

the performance of Hlt2Topo2Body alone. This line requires only two of the three decay tracks of $B^+ \to J/\psi K^+$ to have been reconstructed and selected. Adding Hlt2Topo3Body mainly recovers efficiency at low p_T compared to the Hlt2Topo2Body line alone.

Table 9 lists the cuts applied in the two HLT2 exclusive lines Hlt2CharmHadD02HH_D02KPi and Hlt2CharmHadD2HHH. The off-line selections of $D^0 \to K^- \pi^+$ are only slightly tighter than the cuts applied in HLT2, resulting in an almost maximum efficiency of the

Table 9. HLT2 selection cuts applied for the exclusive lines `Hlt2CharmHadD02HH_D02KPi` and `Hlt2CharmHadD2HHH`. The 2-track cuts refer to a candidate constructed of two tracks, and $m_{\rm corr}$ is defined in equation (3.1). The angle α is the angle between the momentum of the D and the vector connecting the PV with the D vertex. Some selections require that at least one or two tracks pass a cut, indicated with "$\geqq$".

Variable	`Hlt2CharmHadD02HH_D02KPi`	`Hlt2CharmHadD2HHH`
$\chi^2_{\rm track}/{\rm ndf}$	< 3	< 3
Track p_T [MeV/c]	> 800	> 250
Track p [MeV/c]	> 5000	> 2000
Track Σp_T [MeV/c]	$-$	> 2500
$\geqq 1$ track p_T [MeV/c]	> 1500	$-$
2-track mass [MeV/c^2]	$-$	< 2100
2-track $m_{\rm corr}$ [MeV/c^2]	$-$	< 3500
2-track IPχ^2	$-$	> 40
$\geqq 2$ tracks p_T [MeV/c]	$-$	> 500
$\geqq 2$ tracks p [MeV/c]	$-$	> 5000
Track IPχ^2	> 9	> 5
$\geqq 2$ tracks IPχ^2	$-$	> 10
2-track DOCA [mm]	$-$	< 0.1
$\chi^2_{\rm vertex}/{\rm ndf}$	< 10	< 20
FDχ^2	> 40	> 150
D IPχ^2	$-$	< 12
$D \cos(\alpha)$	> 0.99985	$-$
D p_T [MeV/c]	> 2000	> 1000
D mass interval [MeV/c^2]	1815–1915	1800–2040
Rate [Hz]	260	390

`Hlt2CharmHadD02HH_D02KPi` line for this channel, as shown in figure 11. This figure also shows the performance of `Hlt2CharmHadD2HHH` for $D^+ \rightarrow K^- \pi^+ \pi^+$. Here HLT2 loses efficiency due to the necessity of first having to apply hard cuts to two of the three decay products before allowing an extra reconstruction step for low p_T tracks, as described in section 3.2.3.

6 Summary

The LHCb trigger is designed to select charm and beauty hadrons in a large range of decay modes, and permits the measurement of its efficiency directly from data. In 2011 the trigger has been tuned to cope with pp interactions at $\sqrt{s} = 7\,$TeV, with 1296 colliding bunches in LHCb and an average number of visible pp interactions per bunch crossing of 1.4. This corresponds to a bunch crossing rate with at least one visible pp interaction of $\sim 11\,$MHz.

L0 reduces this rate to 870 kHz by applying p_T cuts on muons and E_T cuts on clusters in the calorimeters. HLT1 performs a partial reconstruction of tracks and performs muon identification.
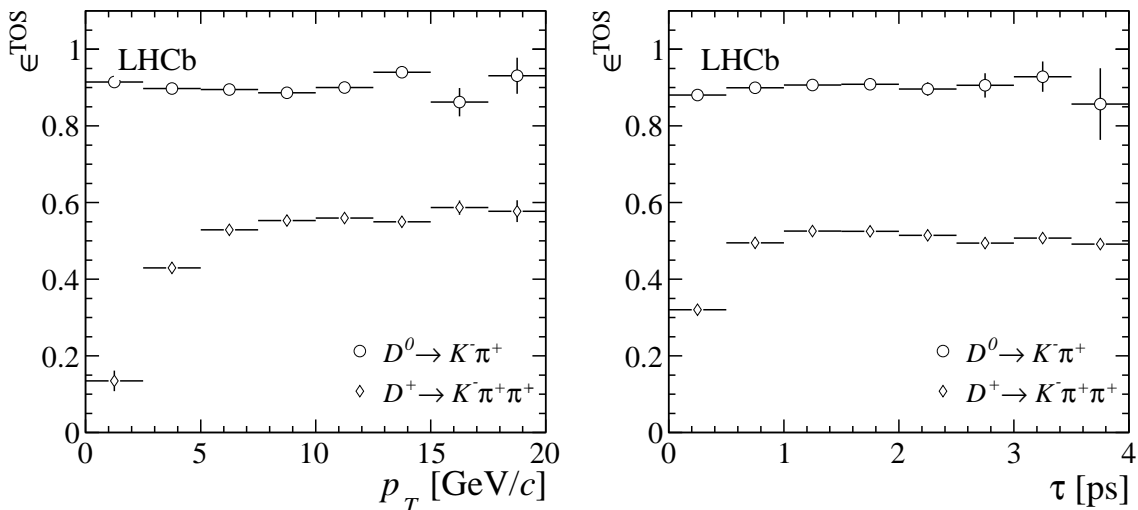
Figure 11. Efficiency ε^{TOS} of the lines `Hlt2CharmHadD2HHH` and `Hlt2CharmHadD02HH_D02KPi` for $D^+ \rightarrow K^-\pi^+\pi^+$ and $D^0 \rightarrow K^-\pi^+$ respectively as a function of p_T and τ of the D-meson. The efficiency is measured relative to events that are TOS in `Hlt1TrackAllL0`.

It employs a combination of cuts on p_T, invariant mass and IP to reduce the rate to around 43 kHz. HLT2 reconstructs all tracks in the event with $p_T > 500 \, \text{MeV}/c$. It selects candidates based on lepton identification, lifetime information and invariant mass. Its output rate is 3 kHz, consisting of 50% inclusive hadronic triggers, 25% triggers on leptons and the remaining rate from exclusive triggers, mainly on charmed hadrons. The efficiencies for the major trigger lines are presented for representative decay modes as a function of p_T and lifetime of c and b-hadrons.

The successful exploitation of the LHC as a beauty factory relies crucially on the ability to trigger on heavy flavour decays in a hadronic environment. To achieve this, the trigger is designed to be able to determine the impact parameter of tracks at a high rate, and to measure the momentum of those tracks with sufficiently large impact parameter, or to identify them as muon candidates. The trigger managed to adapt to the larger pile-up conditions imposed by the machine delivering only 1296 instead of the planned 2622 colliding bunches in the LHC. The trigger performance and the fact that its efficiency can be evaluated in a data-driven way, in combination with the excellent performance of the sub-detectors, allowed LHCb to publish more than 40 papers based on the data collected in 2011.

LHCb is preparing to upgrade the detector [11] in 2018. It will feature a fully software based trigger that will allow it to explore its physics goals at even larger luminosities.

Acknowledgments

References

[1] LHCB collaboration, *The LHCb detector at the LHC*, 2008 *JINST* **3** S08005.

[2] O. Brüning et al., *LHC design report*, CERN-2004-003 (2004).

[3] G. Corti et al., *Software for the LHCb experiment*, *IEEE Trans. Nucl. Sci.* **53** (2006) 1323.

[4] LHCB collaboration, *Roadmap for selected key measurements of LHCb*, arXiv:0912.4179.

[5] LHCB collaboration, *Absolute luminosity measurements with the LHCb detector at the LHC*, 2012 *JINST* **7** P01010.

[6] R.E. Kalman, *A new approach to linear filtering and prediction problems*, *Trans. ASME J. Bas. Eng.* **D 82** (1960) 35;
R. Frühwirth, *Application of Kalman filtering to track and vertex fitting*, *Nucl. Instrum. Meth.* **A 262** (1987) 444.

[7] M. Gandelman and E. Polycarpo, *The performance of the LHCb muon identification procedure*, LHCb-2007-145, CERN-LHCb-2007-145 (2008).

[8] SLD collaboration, *Measurement of R_b using a vertex mass tag*, *Phys. Rev. Lett.* **80** (1998) 660 [hep-ex/9708015].

[9] L. Brieman, J.H. Friedman, R. Olshen and C.J. Stone, *Classication and regression trees*, Wadsworth International Group, Belmont U.S.A. (1984);
L. Breiman, *Bagging predictors*, *Mach. Learn.* **24** (1996) 123;
H.-J. Yang, B.P. Roe and J. Zhu, *Studies of boosted decision trees for MiniBooNE particle identification*, *Nucl. Instrum. Meth.* **A 555** (2005) 370 [physics/0508045].

[10] M. Feindt and U. Kerzel, *The NeuroBayes neural network package*, *Nucl. Instrum. Meth.* **A 559** (2006) 190.

[11] LHCB collaboration, *Letter of intent for the LHCb upgrade*, CERN-LHCC-2011-001 (2011).